Thermal boundary conductance accumulation and interfacial phonon transmission: Measurements and theory

Ramez Cheaito, John T. Gaskins, Matthew E. Caplan, Brian F. Donovan, Brian M. Foley, Ashutosh Giri, John C. Duda, Chester J. Szwejkowski, Costel Constantin, Harlan J. Brown-Shaklee, Jon F. Ihlefeld, and Patrick E. Hopkins

Thermal boundary conductance accumulation and interfacial phonon transmission: measurements and theory

Ramez Cheaito,[1, *] John T. Gaskins,[1, *] Matthew E. Caplan,[1] Brian F. Donovan,[1] Brian M. Foley,[1] Ashutosh Giri,[1] John C. Duda,[1, 2] Chester J. Szwejkowski,[1] Costel Constantin,[3] Harlan J. Brown-Shaklee,[4] Jon F. Ihlefeld,[4] and Patrick E. Hopkins[1, †]

[1]*Department of Mechanical and Aerospace Engineering,*
University of Virginia, Charlottesville, Virginia 22904, USA
[2]*Current address: Seagate Technology, Bloomington, MN 55435, USA*
[3]*Department of Physics and Astronomy, James Madison University, Harrisonburg, VA 22807, USA*
[4]*Electronic, Optical, and Nanomaterials Department, Sandia National Laboratories, Albuquerque, NM 87185, USA*

The advances in phonon spectroscopy in homogeneous solids have unveiled extremely useful physics regarding the contribution of phonon energies and mean free paths to the thermal transport in solids. However, as material systems decrease to length scales less than the phonon mean free paths, thermal transport can become much more impacted by scattering and transmission across interfaces between two materials than the intrinsic relaxation in the homogeneous solid. To elucidate the fundamental interactions driving this thermally-limiting interfacial phonon scattering process, we analytically derive and experimentally measure a thermal boundary conductance accumulation function. We develop a semi-classical theory to calculate the thermal boundary conductance accumulation function across interfaces using the diffuse mismatch model (DMM), and validate this derivation by measuring the interface conductance between eight different metals on native oxide/silicon substrates and four different metals on sapphire substrates. Measurements were performed at room temperature using time-domain thermoreflectance and represent the first-reported values for interface conductance across several metal/native oxide/silicon and metal/sapphire interfaces. The various metal films provide a variable bandwidth of phonons incident on the metal/substrate interface. This method of varying phonons' cutoff frequency in the film while keeping the same substrate allows us to mimic the accumulation of thermal boundary conductance and thus provides a direct method to experimentally validate our theory. We show that the accumulation function can be written as the product of a weighted average of the interfacial phonon transmission function and the accumulation of the temperature derivative of the phonon flux incident on the interface; this provides the framework to extract an average, spectrally dependent phonon transmissivity from a series of thermal boundary conductance measurements. Our approach provides a platform for analyzing the spectral phononic contribution to interfacial thermal transport in our experimentally measured data of metal/substrate thermal boundary conductance. Based on the assumptions made in this work and the measurement results on different metals on native oxide/silicon and sapphire substrates, we demonstrate that high frequency phonons dictate the transport across metal/Si interfaces, especially in low Debye temperature metals with low cutoff frequencies. ~~thermal transport across the solid interfaces is may not necessarily be dictated by phonon mismatch of materials and interfacial transmission, but is rather directly correlated to the temperature derivative of phonon flux incident on the interface.~~

I. INTRODUCTION

Solid-solid interfaces can dominate the thermal processes of devices and material systems when the interface spacing becomes less than the carrier mean free path. This has pronounced effects on thermal transport in nanosystems,[1–3] as the rate of energy transmission across the interface between two solids is often less than the intrinsic rate of conduction in the solids. In fact, even the near-interface regions in a solid can lead to additional thermal resistance due to growth bi-products, atomic imperfections, chemical impurities, and other "non-idealities".[4] Although only a few studies have presented experimental measurements of the thermal boundary conductance across atomically smooth, chemically abrupt interfaces,[5–7] even these works have shown that heat transport across these seemingly "perfect" interfaces can still generate a significant source of thermal resistance.

Even with this thermal boundary conductance (or Kapitza conductance),[8] h_{K}, being immensely important to nanoscale thermal engineering of solids, a void exists in the current knowledge of how phonons interact at interfaces and spectrally contribute to h_{K}. For example, measurements of thermal boundary conductance are typically compared to semi-classical models, such as the acoustic or diffuse mismatch models (AMM or DMM, respectively)[9–11] to analyze how phonons are contributing to interfacial transport. However, due to the many assumptions inherent in these models, agreement between the model predictions and experimental data can often be argued as coincidental. This being said, several previous works, including our own, have developed refinements to the AMM and DMM to garner further insight into how phonon energies are transmitted across solid interfaces.[12–28] Limitations imposed by the fundamental kinetic theory assumptions in which the AMM and DMM are rooted can still raise questions when simply comparing to experimental data.[29] More rigorous classical molecular dynamics simulations have addressed several unanswered questions regarding phonon scattering and subsequent energy transfer across interfaces,[30–49] however, these simulations can not account for quantum mechanical phonon populations below a material's Debye temperature. As a result, the current understanding of how phonons couple and transmit energy across interfaces at moderate temperatures is limited by the mismatch theories or their variants.

Due to these theoretical limitations, knowledge of the physics driving phonon thermal boundary conductance across solid interfaces has lagged considerably compared to the comprehension of phonon scattering processes in homogeneous media. Recent theoretical,[50,51] computational[52–55] and experimental[56–61] works have established the basis of an "accumulation function" for thermal conductivity in homogeneous solids, which has resulted in substantial advances in understanding how phonons scatter and transport energy. This accumulation function provides a direct relationship between carrier mean free path and thermal energy transferred in a solid.

Clearly, a "thermal boundary conductance accumulation function" would substantially advance the field of phonon transport across interfaces, in nanosystems, and through composite media. Although this accumulation function can be easily calculated from the semi-classical mismatch theories, as shown below, an experimental measurement of this accumulation function will provide direct insight into phonon transmission across interfaces. Furthermore, an experimental measurement of this thermal boundary conductance accumulation would provide direct validation of the fundamental assumptions in theories for h_{K} while providing a measure of how phonons are spectrally transmitting across solid interfaces.

In this work, we report on a series of theoretical advancements and experimental measurements that provide evidence into how phonons transmit energy across solid interfaces at room temperature. In doing so, we directly assess the validity of the assumptions of phonon transmission calculations in the DMM. First, we analytically define the thermal boundary conductance accumulation function, and derive this accumulation function assuming diffusive scattering, one of the fundamental assumptions of the DMM. To validate this theory, we measure the thermal boundary conductance across interfaces of eight different metal films and silicon substrates with a native oxide layer. Our experiments show that for native oxide/silicon interfaces, the assumptions of the DMM are acceptable for describing interfacial phonon transmission. Additionally, we further support this assertion through a similar series of measurements on four different metal/sapphire interfaces.

This work provides experimental measurements that give insight into the spectral nature of phonon transport across interfaces. Several previous works have computationally[31,62] and experimentally[63–65] shown that h_{K} across solid/solid interfaces increases with an increase in phonon spectral overlap. However, this does not differentiate between the changing phonon energy flux and transmission probability as the phonon spectra is modified. In this current work, our experimental approach is to keep the substrate constant while changing the metal film deposited on the substrate surface.

We show that with a carefully designed experimental approach, a series of metal/substrate interfaces with different metals can be used as a measure of the spectral accumulation of phonon transmission into the substrate and accumulation of phonon thermal boundary conductance. Furthermore, the data we report provides benchmark values for various transition metal/native oxide/silicon thermal boundary conductances that currently do not exist in the literature. Our choice of various transition metals ensures that the metal/native oxide/silicon interface is well bonded so our results are not affected by weak interfacial adhesion.[66–68] In doing so, we also report on the effects of a Ti adhesion layer between Au and native oxide/Si substrates and show that Ti layers as thin as 2 nm still exhibit thermal boundary conductances that are more in line with a "thick" Ti/Si interface. As a final result of our work, we show that regardless of the metal transducer, we are able to consistently measure the thermal conductivity of a single crystalline silicon substrate in agreement with bulk literature values within the experimental uncertainty.[69–71] This further validates time-domain thermoreflectance (TDTR) as an effective measurement tool for measuring the thermal conductivity of bulk materials.

II. ACCUMULATION OF THERMAL BOUNDARY CONDUCTANCE

A simplistic mathematical description of phonon thermal boundary conductance from side 1 to side 2 is given by:

$$h_{\mathrm{K}} = \sum_j \int_{\omega_{\min,j}}^{\omega_{\max,j}} \frac{\partial q_{1,j}(\omega)}{\partial T} \zeta_{1\rightarrow 2}(\omega)\,\mathrm{d}\omega \tag{1}$$

where ω is the phonon angular frequency in rad s^{-1}, T is the temperature, $\zeta_{1\rightarrow 2}$ is the phonon transmission coefficient from side 1 to side 2, $\omega_{\min,j}$ and $\omega_{\max,j}$ are the minimum and maximum frequencies in branch j, respectively, and $q_{1,j}$ is the spectral phonon flux in side 1 of phonon polarization j, where the temperature derivative of this phonon flux is defined as:

$$\frac{\partial q_{1,j}(\omega)}{\partial T} = \frac{1}{4}\hbar\omega \mathcal{D}_{1,j}(\omega)\, \upsilon_{1,j}(\omega) \frac{\partial f(\omega)}{\partial T} \tag{2}$$

where $\hbar$ is Plank's constant divided by 2π, f is the Bose-Einstein distribution at equilibrium, and $\mathcal{D}_{1,j}$ and $\upsilon_{1,j}$ are the density of states and phonon group velocity in side 1, respectively. We can absorb the branch dependence into the integral by rewriting the equation as:

$$h_{\mathrm{K}} = \int_{\omega_{\min}}^{\omega_{\max}} \frac{\partial q_1(\omega)}{\partial T} \zeta_{1\rightarrow 2}(\omega)\,\mathrm{d}\omega \tag{3}$$

where $\omega_{\max} = \max(\omega_{\max,j})$, $\omega_{\min} = \min(\omega_{\min,j}) = 0$ and $\partial q_1(\omega)/\partial T$ is given by:

$$\frac{\partial q_1(\omega)}{\partial T} = \sum_j \frac{\partial q_{1,j}(\omega)}{\partial T} \ \text{with} \ \frac{\partial q_{1,j}(\omega)}{\partial T}\bigg|_{\substack{\omega>\omega_{\max,j}\\ \omega<\omega_{\min,j}}} = 0 \tag{4}$$

Equation 3 expresses h_{K} as a product of two functions: the temperature derivative of the phonon flux and the phonon transmission coefficient. In parallel to previous theoretical works on thermal conductivity accumulation,[50,51] we can now define a thermal boundary conductance accumulation, α_{K}, as:

$$\alpha_{\mathrm{K},1\rightarrow 2}(\omega_\alpha) = \frac{1}{h_{\mathrm{K}}} h_{\mathrm{K},1\rightarrow 2}(\omega_\alpha) \tag{5}$$

where

$$h_{\mathrm{K},1\rightarrow 2}(\omega_\alpha) = \int_0^{\omega_\alpha} \frac{\partial q_1(\omega)}{\partial T} \zeta_{1\rightarrow 2}(\omega)\,\mathrm{d}\omega = \int_0^{\omega_\alpha} \mathfrak{h}_{\mathrm{K}}(\omega)\,\mathrm{d}\omega \tag{6}$$

is the un-normalized Kapitza conductance accumulation function and represents the portion of the total thermal boundary conductance due to carriers in the metal (side 1) with phonon frequencies less than ω_α transmitting energy to side 2. The equation on the far right of Eq. 6 recasts the integrand into a spectral thermal boundary conductance, $\mathfrak{h}_{\mathrm{K}}$. Ultimately, this accumulation function is dictated by the product of $\partial q_1/\partial T$ and $\zeta_{1\rightarrow 2}$, both of which are dependent on frequency and therefore difficult to explicitly separate from this integral to compare with experimental data. However, we can separate these quantities using the Generalized Mean Value Theorem for definite integrals[72] which states that there exists a frequency $x \in [0, \omega_\alpha]$ such that:

$$h_{\mathrm{K},1\rightarrow 2}(\omega_\alpha) = \overline{\zeta_{1\rightarrow 2}(x(\omega_\alpha))} \int_0^{\omega_\alpha} \frac{\partial q_1(\omega)}{\partial T}\,\mathrm{d}\omega \tag{7}$$

where $\overline{\zeta_{1\rightarrow 2}(x(\omega_\alpha))}$ is the average of interfacial transmission from side 1 to side 2 over the frequency interval $[0, \omega_\alpha]$ weighted by $\partial q_1/\partial T$. Since ω_α is the independent variable in our formulation, and x is a function of ω_α we can write $\overline{\zeta_{1\rightarrow 2}}$ solely as a function of ω_α so that Eq. 7 becomes

$$h_{\mathrm{K},1\rightarrow 2}(\omega_\alpha) = \overline{\zeta_{1\rightarrow 2}(\omega_\alpha)} Q_T(\omega_\alpha) \tag{8}$$

where $Q_T(\omega_\alpha) = \int_0^{\omega_\alpha} \partial q_1/\partial T \, \mathrm{d}\omega$ is the un-normalized accumulation of $\partial q_1/\partial T$. We also define $\alpha_{qT}(\omega_\alpha)$ as the normalized $Q_T(\omega_\alpha)$. We note that this approach provides the separation of flux and average transmission (which is related to the fundamental mechanisms of phonon scattering and energy transport at interfaces) in the formulation of thermal boundary conductance.
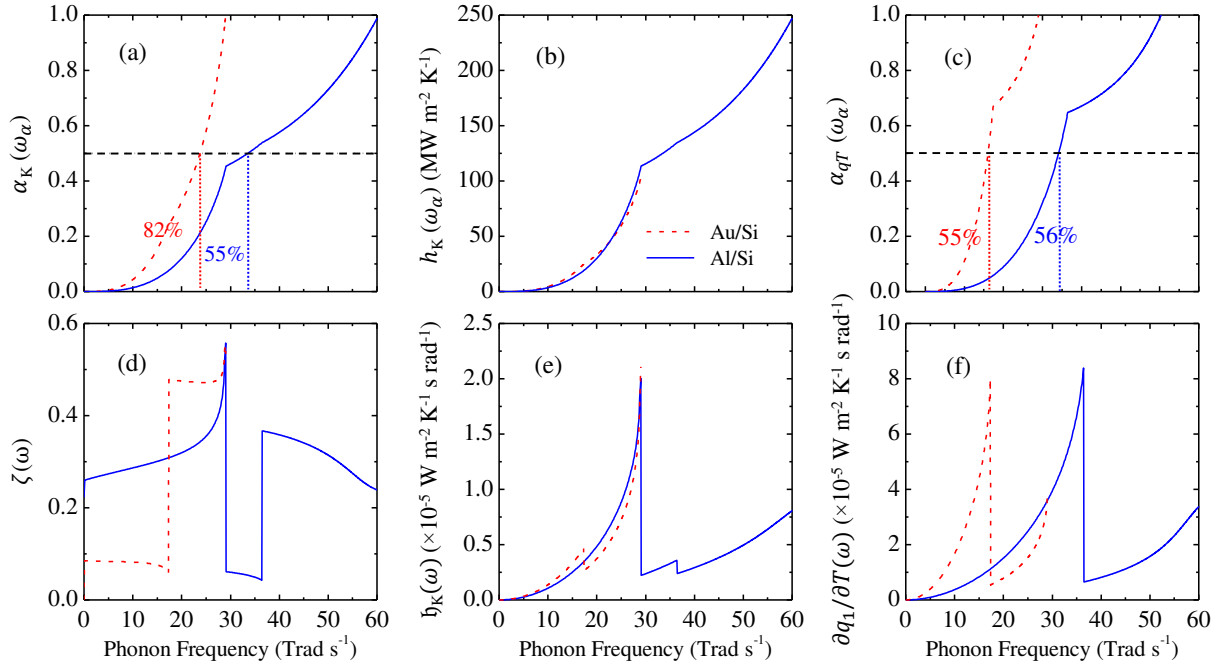
FIG. 1. (a) Thermal boundary conductance accumulation function, $\alpha_K(\omega_\alpha)$, (b) un-normalized thermal boundary conductance accumulation function, $h_K(\omega_\alpha)$, (c) accumulation of the temperature derivative of the phonon flux in the metal, $\alpha_{qT}(\omega_\alpha)$, (d) transmission coefficient, $\zeta(\omega)$, (e) spectral thermal boundary conductance, $\mathfrak{h}_K(\omega)$ and (f) temperature derivative of phonon flux in the metal, $\partial q_1/\partial T(\omega)$, for Al/Si (solid line) and Au/Si (dashed line) interfaces as a function of phonon frequency calculated using Eqs. 5- 8 at room temperature. The horizontal line in (a) and (c) designates the portion of the spectrum contributing to 50% of the plotted quantity. The calculations suggest that the majority of heat is carried by high frequency phonons in Au but is more evenly spread across the spectrum in Al. The features in curves are related to the Van Hove singularities[73] in the various phonon spectra and our assumptions in the DMM calculations. Discontinuities in the slopes of the various calculations occur at the frequencies corresponding to the Brillouin Zone edge of either the metal or silicon. Note that for Al/Si accumulation in (a) and (b), there is a very slight second discontinuity in the trend of $h_K(\omega_\alpha)$ at the Al TA cutoff frequency of 36.4 Trad s^{-1}, which can be observed more clearly in the $\mathfrak{h}_K(\omega)$ in (e). The various modeling calculations shown in these plots and the MATLAB code used to generate these accumulation models are given in the supplementary materials.[74]

We show example calculations of the different variables given in Eqs. 5- 8 in Fig. 1 for Al/Si and Au/Si interfaces using DMM assumptions. This assumption of diffusive phonon scattering directly impacts calculations of the phonon transmissivity but not the calculations of the metal phonon flux. These assumptions and our specific procedure for the DMM are outlined in detail in our previous works, and are not repeated here.[75,76] For these calculations, we ignore the contribution from optical modes and assume a 4th order polynomial fit to the one-dimensional phonon dispersion in the $\Gamma \rightarrow X$ direction in Au (Ref. 77), Al (Ref. 78), and Si (Ref. 79), and an isotropic Brillouin zone, which is an acceptable approximation for cubic structures.[80] Finally, we assume two-phonon elastic scattering as the mechanism for phonon transmission across interfaces,[20,21] and therefore we only conduct these calculations up to the maximum phonon frequencies in the metal which corresponds to the cutoff frequency of the longitudinal acoustic branch (e.g., frequencies above $\sim$30 Trad s^{-1} in Au are assumed to not contribute to h_K). The dispersion curves used for this calculation are shown in Fig. 2(a) for aluminum on silicon denoted by "Real Dispersion". The shaded area in the figure represents the $k - \omega$ space over which the integration is carried when $\omega_\alpha = 40$ Trad s^{-1}, where k is the wavevector. In this case, the integration is carried over a subset of the Brillouin zone in the metal. Points A' and B' on the shaded region will coincide with A and B on the solid rectangle when $\omega_\alpha = \omega_{max}$. Note that the integration limits correspond to the angular frequency vector describing the longitudinal acoustic (LA) branch in the metal as the cutoff frequency of this branch is higher than that in the transverse acoustic (TA). The accumulation of thermal boundary conductance α_K and the un-normalized accumulation, $h_K(\omega_\alpha)$, for Al/Si and Au/Si interfaces, calculated with Eqs. 5 and 6 are plotted in Fig. 1a and b. Figure 1b shows that Kapitza conductance is 250.1 MW m^{-2} K^{-1} and 102.9 MW m^{-2} K^{-1} across Al/Si and Au/Si interfaces, respectively. The differing values for thermal boundary conductance are a function of the metal film flux and maximum phonon frequency in the metal, which drives the total phonon energy incident on the interface. The value for Au/Si agrees to within 83% with the DMM calculations by Dechaumphai $et\ al.$[81] using a three-dimensional real dispersion. This agreement suggests that the use of a one-dimensional realistic dispersion along the $\Gamma \rightarrow X$ direction is an acceptable approximation. Up to the cutoff frequency of the Au, $h_K(\omega_\alpha)$ for Au/Si and Al/Si are nearly identical. This can also be seen in the spectral Kapitza conductance, $\mathfrak{h}_K(\omega)$,
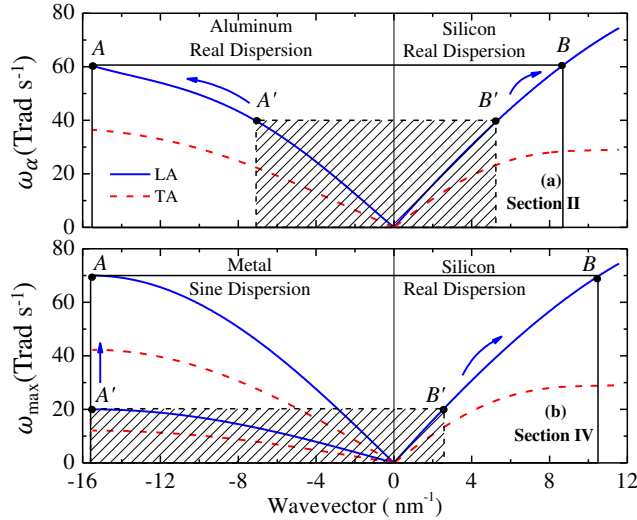
FIG. 2. (a) The dispersion curves used in the calculation of $\alpha_{K,1\to2}$ in Eqs. 6 & 8 for Al/Si and plotted in Fig 1. The shaded area represents the $k - \omega$ space over which the integration is carried when $\omega_\alpha = 40$ Trad s^{-1}. Points A' and B' on the shaded region will coincide with A and B on the solid rectangle when $\omega_\alpha = \omega_{\max}$ where both points will move along the longitudinal acoustic branch (LA) in aluminum and silicon, respectively. (b) The dispersion curves used in the calculation of $h_K\left(v_1\left(\omega_{\max}\right)\right)$ given by Eq. 10 for metal/Si and plotted in Fig. 4. The shaded area represents the $k - \omega$ space over which the integration is carried when $\omega_{\max} = 20$ Trad s^{-1} and $v_1\left(\omega_{\max}\right)$ is given by the dispersion curves contained within the shaded region. Points A' and B' will coincide with A and B and the dispersion curves in the shaded region will coincide with the dispersion curves in the solid rectangle when $\omega_{\max} = 70$ Trad s^{-1} with point B' moving along the LA branch in silicon and point A' moving vertically along the left side of the solid rectangle. The blue arrows denote the movement direction of the vertices of the shaded region as the angular frequency increases.

plotted in Fig. 1e. The trend in the accumulation function follows the trend in the accumulation of the temperature derivative of the phonon flux, $\alpha_{qT}(\omega_\alpha)$, plotted in Fig. 1c. The TA cutoff frequency in Si is almost equal to the maximum cutoff frequency in Au (~ 29 Trad s^{-1}), but smaller than the TA and LA cutoff frequencies in Al, 36.4 and 60 Trad s^{-1}, respectively. As a result, transport across Al/Si is more affected by higher frequency modes in the Si as compared to Au/Si as ω_α crosses the TA cutoff frequencies in Al and Si. This influence of mode cutoff frequencies appears as singularities at these two frequencies in the different variables plotted in Fig. 1 and leads to the clear degradation in the slope of $h_K(\omega_\alpha)$ for Al/Si for frequencies higher than 29 Trad s^{-1}. This degradation in the slope can be interpreted in terms of the portion of the spectrum contributing to Kapitza conductance. The vertical and horizontal lines in Fig. 1a show that 50% of the Kapitza conductance across Au/Si and Al/Si interfaces is dictated by 82% and 55% of the phonon spectrum in Au and Al, respectively. In other words, across the Au/Si interface, high frequency modes in the Au are carrying 50% of the heat, while across the Al/Si interface, interfacial phonon transport is more evenly distributed across all the modes in the Al. Applying the same analysis to $\alpha_{qT}(\omega_\alpha)$, the accumulation of the $\partial q/\partial T$, in Fig. 1c shows that the phonon flux incident upon the interface is evenly distributed across the metallic spectrum for both systems. However, the transmission coefficient for Al/Si plotted in Fig. 1d shows a clear drop and a decreasing trend at frequencies higher than 29 Trad s^{-1} while it shows a relatively flat trend over the entire frequency range for Au/Si. This leads to the first conclusion in our work: the phononic mismatch between the two materials on either side of the interface influences the spectral contribution to the phonon transmission across interfaces. While the phonon flux dictates the magnitude of the Kapitza conductance in a certain system, the transmission coefficient directly affects the phonon frequencies at which energy is trans-ferred across the interface. ~~The similarity between the Al/Si and Au/Si curves implies that the frequency trends in accumulation of phonon thermal boundary conductance at a metal/Si interface is a direct function of the silicon properties.~~

~~More insight into these trends is gleaned by considering the calculations of Eq. 6. We plot $\alpha_{K,1\to2}$ and the normalized accumulation of $\partial q_1/\partial T$ here denoted by α_{qT} for Au/Si and Al/Si in Figs. 1b and c, respectively. The accumulation of both flux and interface conductance predictions for Au/Si and Al/Si have very similar shapes. While q_1 (and therefore $\partial q_1/\partial T$) is an intrinsic property of the material and can be relatively well predicted from accurate phonon dispersion relations without any assumptions of the interfacial scattering mechanisms, $\zeta_{1\to2}$ relies heavily on the nature of phonon scattering and energy transfer across interfaces.[75] For example, in the discussion above, we implemented the assumptions of the DMM in our calculations, which directly impacted our calculation of $\zeta_{1\to2}$. However, this is simply an assumption, and we will now turn to experimental measurements to gain more insight into the nature of phonon scattering and energy transmission across solid interfaces.~~

The definition of Kapitza conductance accumulation given in this section follows the mathematical definition of accumula-tion functions and uses the same approach used for defining the thermal conductivity accumulation function in recent publi-

cations.[50,51] The results of this section have implications on the interpretation of experimental thermal boundary conductance measurements. However, this approach is not helpful to compare experimental data to theoretical predictions as there is currently no straightforward, robust method to measure Kapitza conductance across a specific metal/substrate interface up to a specific phonon frequency lower than the metal cutoff frequency. As a result, we use an alternative theoretical approach to mimic the Kapitza conductance accumulation, discussed in Section IV. This approach allows for direct comparison with experimental measurements presented in Section III.

III.   TDTR MEASUREMENTS OF THERMAL BOUNDARY CONDUCTANCE

Experimental measurements of the phonon transmission coefficient driving thermal boundary conductance at non-cryogenic temperatures do not exist,[82] and insight into the fundamental assumptions and processes of $\zeta_{1\to2}$ at elevated temperatures would greatly advance phonon interfacial physics and heat transfer. In the work that follows, we use the analyses and results presented in Fig. 1 to extract the thermal boundary conductance accumulation and phonon transmissivity from experimental measurements of h_{K} across metal/native oxide/silicon and metal/sapphire interfaces. By varying the metal while keeping the substrate otherwise identical, we change the "phonon flux" term, which changes the maximum frequency in the metal and the accessible modes in the substrate that couple to the metal phonons. With relation to Fig. 1, by changing the metal film, we incrementally increase the phonon frequency on the accumulation curve (i.e., the metal film systematically changes the maximum value of ω_α in Eq. 6). This approach yields direct insight into the mechanisms of phonon transmissivity into the substrate, as we describe in the remainder of this work.

We design a series of experiments to investigate $\overline{\zeta_{1\to2}(\omega_\alpha)}$ via measurements related to the thermal boundary conductance accumulation function ($\alpha_{\mathrm{K},1\to2}$, Eq. 8). Without having to make any assumptions about how the phonons scatter at the interface, $\mathfrak{h}_{\mathrm{K}}$ is directly related to both the phonon transmission coefficient and the temperature derivative of the phonon flux in side 1. To a first approximation (i.e., no extreme temperature gradients),[38,83,84] in a homogeneous material, $\partial q_1(\omega)/\partial T$ is easily calculated from knowledge of the phonon dispersion relations. With this, a consistent set of measurements can probe $\overline{\zeta_{1\to2}(\omega_\alpha)}$, the interplay between phonon flux and transmission contributions to thermal boundary conductance, and the accumulation of phonon thermal boundary conductance.

Our experimental approach is based around measurements of h_{K} on a series of metal films on (001)-oriented silicon substrates with a native oxide layer; in this case, q_1 is well defined by the phonon dispersion and well known lattice heat capacities in the metal, while $\overline{\zeta_{1\to2}(\omega_\alpha)}$ is contained in our measurements by comparing to calculations of $\partial q_1(\omega)/\partial T$. We use consistent cleaning procedures on our substrates (alcohol and oxygen plasma clean) to ensure similar surface conditions upon metal evaporation. Various metal films were sputtered or evaporated at both Sandia National Laboratories and the University of Virginia, where several of each type were repeated at each institution to ensure consistency in our reported data. Several previous works have measured h_{K} across a select few metal/native oxide/silicon interfaces.[64,66,85–88] We report on measurements with nearly identical silicon surfaces to avoid effects due to contamination and surface roughness.[4,87,89–91]

We measured the thermal boundary conductance using time domain thermoreflectance (TDTR), which is well suited to measure h_{K}.[4,92–94] In our experiments, we use a modulation frequency of 8.81 MHz and a pump and probe $1/e^2$ radii of 35 and 12 μm, respectively. To minimize uncertainty, we measure the metal film thickness with a combination of profilometry, white light interferometry, atomic force microscopy, and when possible, picosecond acoustics.[95] We fit widely used thermal models derived for TDTR to our experimental data using both h_{K} and the substrate thermal conductivity as free parameters.[92,93] As a calibration of our measurements, we report the best fit silicon thermal conductivity as a function of the metal film Debye temperature[100] in Fig. 3a. Regardless of metal film, we measure the thermal conductivity of silicon within the uncertainty of the range of literature values for bulk silicon.[69,70,96–99] This not only gives further confidence to our reported values, but also shows that TDTR is a suitable experimental technique to measure the thermal conductivity of bulk Si. We caution that we used large pump and probe spot sizes to avoid radial spreading effects,[60] and in spite of operating at a relatively high modulation frequency for TDTR,[56,58] we were able to accurately measure the thermal conductivity of the silicon substrates. Relatively large spot sizes must be employed if attempting to accurately measure the thermal conductivity of a bulk substrate, especially substrates with relatively high thermal effusivities, as pointed out in a recent work by Wilson and Cahill.[101]

The thermal boundary conductances across the metal/native oxide/Si interfaces as a function of metal Debye temperature are shown in Fig. 3b. For the most part, our data and trends with metal Debye temperatures agree well with the previously reported values (open symbols).[64,85–88] We will examine this in terms of phonon accumulation and transport physics in the next section, however, we note that these data provide first-reported values for h_{K} across several transition metal/native oxide/Si interfaces, which are important for an array of applications due to the wide spread use of silicon and metallized silicon contacts.

As another aside, it is interesting to note that the inclusion of Ti adhesion layers between Au and native oxide/Si increases the thermal boundary conductance substantially, as we have reported recently.[66] We tested 3 different Au/Ti/native oxide/Si samples with different Ti thicknesses (2, 15, and 40 nm). Within experimental uncertainty, we measure the same thermal boundary conductance for each sample. The very similar agreement among the 2, 15 and 40 nm Ti cases suggests that the phonons in Ti play a role in h_{K} at thicknesses as small as 2 nm.
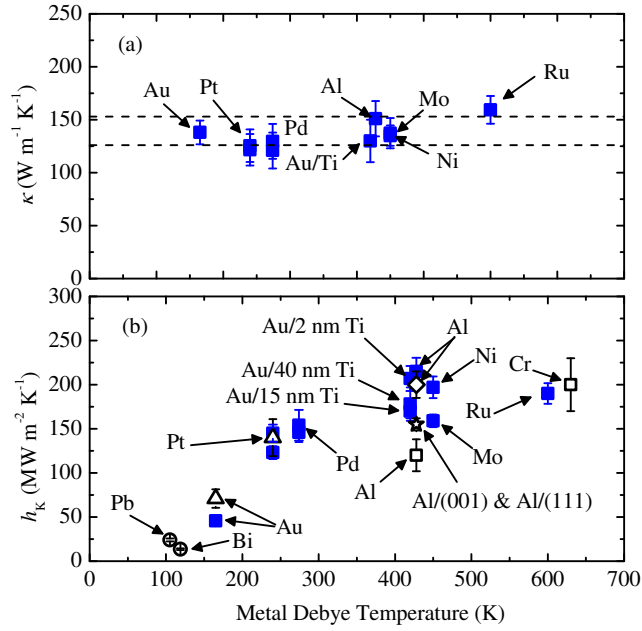
FIG. 3. (a) Thermal conductivity of the silicon substrates coated with various metal films measured with TDTR. The dotted lines represent the range of accepted values for thermal conductivity of bulk silicon.[69,70,96–99] (b) Thermal boundary conductance across the metal/native oxide/Si interfaces as a function of metal Debye temperature. The data reported in this work are shown as filled symbols while previously reported results are depicted as open symbols (Bi and Pb: Ref. 88; Au, Pt, Al, and Cr: Ref. 64; Al/(001) and Al/(111): Ref. 85; Al: Ref. 86). The thermal boundary conductance data are tabulated in the supplementary materials.[74]

IV. ANALYSES OF EXPERIMENTAL DATA AND PHONON TRANSMISSION COEFFICIENT ACROSS METAL/NATIVE OXIDE/SILICON AND METAL/SAPPHIRE INTERFACES

We can now analyze the data in Fig. 3b to quantify various aspects of thermal boundary conductance accumulation. The different metal films' cutoff frequencies vary between 13.5 and 60 Trad s^{-1}. This provides a varying "bandwidth" of phonons that are incident on the metal/native oxide/silicon interface, where each metal has a corresponding dispersion curve defined over the entire metal Brillouin zone and of maximum cutoff frequency less than or equal to 60 Trad s^{-1}. However, the formulation in Section II derives the accumulation of Kapitza conductance assuming a single dispersion in the metal side. As a result, we can not directly compare the measurement results on Kapitza conductance to the accumulation function defined earlier. Instead, we reformulate the accumulation function to account for the varying dispersion relation by making h_{K} a function of the phonon group velocity in side 1. In the most general case Eq. 1 is rewritten:

$$h_{\mathrm{K}}\left(\omega_{\min,j},\omega_{\max,j},v_{1,j}\left(\omega,\omega_{\min,j},\omega_{\max,j}\right)\right)=\sum_{j}\int_{\omega_{\min,j}}^{\omega_{\max,j}}\frac{\partial q_{1,j}\left(v_{1,j}\left(\omega,\omega_{\min,j},\omega_{\max,j}\right)\right)}{\partial T}\zeta_{1\to2}\left(v_{1,j}\left(\omega,\omega_{\min,j},\omega_{\max,j}\right)\right)\mathrm{d}\omega$$

(9)

where the dependence of $v_{1,j}$ on $\omega_{\min,j}$ and $\omega_{\max,j}$ is to emphasize that while $v_{1,j}$ is dependent on ω, the variable of integration, its domain of definition, $[\omega_{\min,j},\omega_{\max,j}]$, is also variable. Using the same approach as in Section II, we can also separate a weighted average of the transmission coefficient and simplify the above equation to:

$$h_{\mathrm{K}}\left(v_1\left(\omega_{\max}\right)\right)=Q_T\left(v_1\left(\omega_{\max}\right)\right)\overline{\zeta_{1\to2}\left(v_1\left(\omega_{\max}\right)\right)}$$

(10)

where

$$Q_T\left(v_1\left(\omega_{\max}\right)\right)=\int_0^{\omega_{\max}}\frac{\partial q_1\left(v_1\left(\omega_{\max}\right)\right)}{\partial T}\mathrm{d}\omega$$

(11)

and we dropped the dependence on ω and the different cutoff frequencies and set the lower integration limit to zero for simplicity. Defining a generic expression for v_1 and varying the cutoff frequency in the metal allows us to compare $h_{\mathrm{K}}\left(v_1\left(\omega_{\max}\right)\right)$ to

the experimental measurements on different metals. In this case, $h_K\left(\upsilon_1\left(\omega_{\max}\right)\right)$ is the un-normalized Kapitza conductance accumulation across varying metal/Si interfaces. We recall that $\omega_{\max}$ is equal to the LA cutoff frequency in the metal ($\omega_{\max} = \omega_{\max,\mathrm{LA}}^{\mathrm{metal}}$).

In Eq. 10, $h_K\left(\upsilon_1\left(\omega_{\max}\right)\right)$ and $Q_T\left(\upsilon_1\left(\omega_{\max}\right)\right)$ are calculated assuming a Sine-type dispersion for the metal phonons and using the polynomial fitted dispersion for silicon. Assuming a sine-type dispersion in the metal allows us to continuously vary the approximated phonon spectrum in the metal film by simply changing the cutoff frequency in the dispersion calculations,[102] yielding a model input for the metal phonon flux in Eq. 10. The dispersion curves used in this calculation are shown in Fig. 2(b). For these calculations, we assume a ratio of transverse to longitudinal cutoff frequencies in the metal based on the ratio of cutoff frequencies in Al and assume the lattice constant to be that of Al. The solid line in Fig. 4a shows the computed values of $h_K\left(\upsilon_1\left(\omega_{\max}\right)\right)$ at room temperature up to the maximum cutoff frequency in Si along with the data from Fig. 3b. It is important to understand that the model plotted in Fig. 4a is not the mathematically known accumulation function and is thus different from the model plotted in Fig. 1b. However, to a first approximation, the data and model in Fig. 4a "mimic" the accumulated phonon thermal boundary conductance across metal/Si interfaces. In this case, the different metal films change the accumulated frequency, so metal films with higher $\omega_{\max}$ simply increase the frequencies of phonons in silicon that contribute to h_K. The difference between the formulation in this section and that in Section II can be further understood from the difference between the dispersion curves and the $k-\omega$ space over which the integration is carried out, illustrated in Fig. 2. While we used a single dispersion curve for the calculation of $\alpha_K\left(\omega_\alpha\right)$ in Section II, for each point of abscissa $\omega_{\max}$ on the solid line plotted in Fig. 4a, there corresponds a sine-type dispersion curve defined over $[0,\omega_{\max}]$ and over the entire Brillouin zone in the metal side. In Fig. 2(b), the shaded area represents the space over which the integration is carried when $\omega_{\max} = 40$ Trad s^{-1} and $\upsilon_1\left(\omega_{\max}\right)$ is given by the dispersion curve contained within the shaded region. Points A' and B' will coincide with A and B and the dispersion curves in the shaded region will coincide with that in the solid rectangle when $\omega_{\max} = 70$ Trad s^{-1}. Our model prediction for the thermal boundary conductance accumulation shown in Fig. 4a agrees well with our experimental data, especially considering the simplicity of our approach and phonon dispersion assumptions that we used in this procedure. We note that no fitting parameters are used in this model.

The isotropic solid assumption used in the calculation of the DMM is acceptable for cubic structures,[78] however, bulk Ti and Ru have hcp crystal structure and Bi has a rhombohedral structure. Furthermore, thin Ti films can exhibit fcc, hcp, or a mix of hcp and fcc structures as has been shown in Al/Ti bilayers[103] depending on the film thickness. With the lack of literature on the crystal structure of thin Au/Ti bilayers, it is difficult to assess the applicability of the isotropic solid assumption to our Au/Ti/Si samples studied here. However, the agreement between Kapitza conductance measurement on Au/Ti/Si, Bi/Si, and Ru/Si and the other metals with cubic structures over the range of cutoff frequencies may justify this assumption. We also note that while a Sine-type dispersion is valid for simple cubic structures, all the metals measured have fcc, bcc, hcp, or rhombohedral structures. To check this approximation, we compare the Kapitza conductance across Al/Si and Au/Si interfaces using Sine-type and real-type dispersions, where our "real-type" dispersions were discussed in Section II. The result shows that the ratio of Sine to real dispersion Kapitza conductances is 0.96 for Al/Si and 1.04 for Au/Si. Noting the excellent agreement between Sine and real dispersion and the fact that Al and Au have fcc structures, suggest that the use of a Sine dispersion is an acceptable approximation.

The plot in Fig. 4a shows two singularities labeled as S1 and S2. S1 occurs at $\sim$29 Trad s^{-1} when $\omega_{\max}$ reaches the TA cutoff frequency in Si and the second, S2, occurs at $\sim$48 Trad s^{-1} when the TA cutoff frequency in the metal reaches the TA cutoff frequency in Si. S1 and S2 are important in interpreting and understanding the results of the accumulation function. The inset of Fig. 4a shows the normalized model calculations for $Q_T\left(\upsilon_1\left(\omega_{\max}\right)\right)$, denoted by $\alpha_{qT}\left(\upsilon_1\left(\omega_{\max}\right)\right)$, normalized to the values of $Q_T\left(\upsilon_1\left(\omega_{\max}\right)\right)$ at the maximum cutoff frequency (74 Trad s^{-1}). The accumulated temperature derivative of the phonon flux increases monotonically with phonon cutoff frequency, $\omega_{\max}$. Even though this is a prediction from our model, this result is not surprising since to a first approximation, the cutoff frequency of metals with one atomic basis will directly scale with sound velocity and is related to the phonon density of states. At room temperature, the metals considered in this work can be considered in or near the classical limit (even for higher Debye temperature metals, such as Al, as their heat capacities are relatively flat around room temperature, justifying this assumption). In this case, the Bose-Einstein distribution can be estimated by: $f = k_B T/\hbar\omega$. Using the isotropic solid expression for the density of states given by $\mathcal{D}_{1,j}\left(\omega\right) = \omega^2/\left(2\pi^2\upsilon_{1,j}^3\left(\omega\right)\right)$ and invoking the Debye approximation for this analytical example, the phonon flux in the metal can be estimated by: $q_{1,j} = k_B\omega^2 T/\left(8a^2\omega_{\max,j}^2\right)$ where a is the lattice constant in the metal. Carrying out the integration Q_T can be estimated by:

$$Q_T \approx \frac{k_B}{24a^2}\left(\omega_{\max,\mathrm{LA}} + 2\omega_{\max,\mathrm{TA}}\right) = \frac{k_B}{24a^2}(1+2s)\omega_{\max} \tag{12}$$

where $s = \omega_{\max,\mathrm{TA}}/\omega_{\max,\mathrm{LA}}$ is the ratio of the transverse to longitudinal acoustic cutoff frequencies in aluminum used for the calculation shown in Fig. 4 and $\omega_{\max,\mathrm{LA}} = \omega_{\max}$. This approximation explains the origin of the nearly linear behavior in α_{qT} in the inset of Fig. 4.

The Kapitza conductance accumulation, $\alpha_K\left(\upsilon_1\left(\omega_{\max}\right)\right)$, can be calculated by normalizing the model in Fig. 4a to the value of $h_K(\upsilon_1(\omega_{\max}))$ at a certain frequency $\omega_{\max,\mathrm{N}}$, where N denotes normalization. Similar to the analysis in Section II, we use α_K
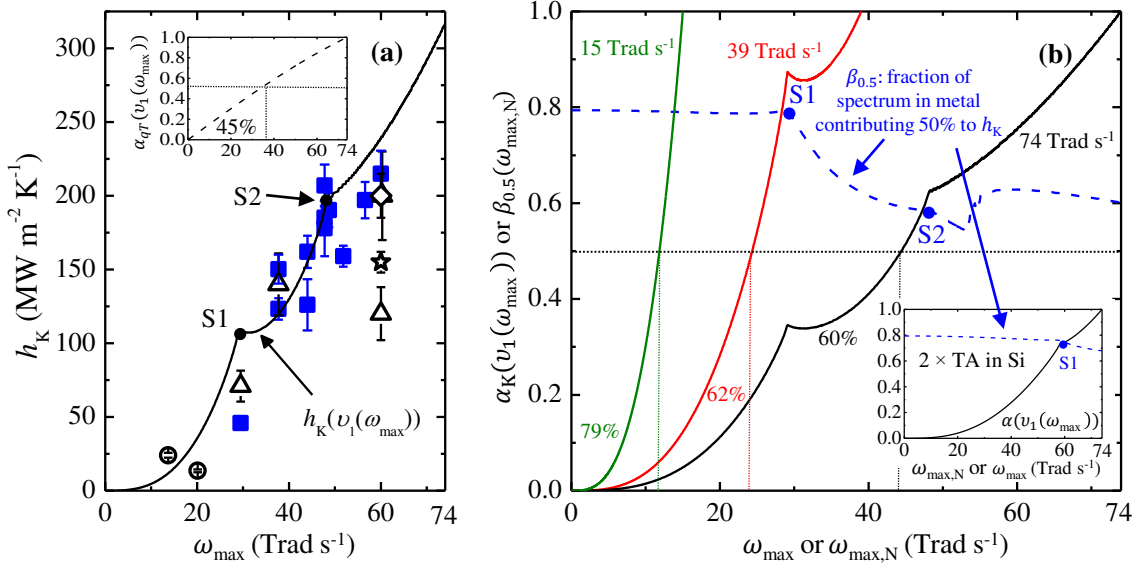
FIG. 4. (a) Measured thermal boundary conductance as a function of metal cutoff frequency (phonon frequencies are taken from phonon dispersion curves in the literature).[77,78,104–112] Our model for thermal boundary conductance as a function of $\omega_{\max}$ agrees well with the data discussed in this work. S1 and S2 denote the two singularities in the calculation of $h_K(\upsilon_1(\omega_{\max}))$. The inset shows the normalized accumulation of the temperature derivative of the phonon flux. The horizontal and vertical lines in the inset show that 50% of the computed value of α_{qT} is dictated by the first 45% of the phonon spectrum. The nearly linear change in α_{qT} with $\omega_{\max}$ implies that the nonlinear features in the measurements and the model can be attributed to the phonon transmissivity across the metal/Si interfaces. (b) Three plots of the thermal boundary conductance accumulation function for metal/Si, $\alpha_K(\upsilon_1(\omega_{\max}))$, obtained by normalizing the solid line in (a) at 15, 39, and 74 Trad s^{-1}. Each of these plots is labeled by the percentage of the phonon spectrum contributing to 50% of the interfacial transport. The dashed line represents $\beta_{0.5}$ plotted as a function of the normalization frequency, $\omega_{\max,N}$. The inset in (b) shows $\beta_{0.5}$ for which the TA branch in Si was multiplied by a factor of 2 and the corresponding $\alpha_K(\upsilon_1(\omega_{\max}))$. We provide the MATLAB code used to generate this accumulation model in the supplementary materials.[74]

to determine the spectral phonon contribution to h_K. Figure 4b shows three plots of $\alpha_K(\upsilon_1(\omega_{\max}))$ normalized at 15, 39, and 74 Trad s^{-1}. It is clear that as the normalization cutoff frequency is increased, the slope of the corresponding accumulation function decreases leading to a reduced role of high frequency phonons. To gain more insight, we define $\beta_x(\omega_{\max,N})$ as the fraction of the phonon spectrum in the metal contributing to x-fraction of the computed value of h_K for a maximum cutoff frequency of $\omega_{\max,N}$. The dashed line in Fig. 4b represents $\beta_{0.5}$ showing the fraction of thermal boundary conductance dictated by the first 50% of the phonon spectrum in metal. The result demonstrates that up to S1, 50% of the heat is carried across the interface by the first 79% of the spectrum. This means that for metals with cutoff frequencies less than the TA cutoff frequency in Si (Pb, Bi, and Au), high frequency phonons (or the upper 21% frequencies in the metals' phononic spectra) are the dominant frequency modes. $\beta_{0.5}$ then decreases after S1 to reach a value of 0.53 at a slightly higher frequency than S2. The trend is followed by an increase as higher frequency phonons are excited in Si and the metal. At around 58 Trad s^{-1}, the system has fully accumulated and $\beta_{0.5}$ takes a relatively constant value of ~0.6.

The trend in $\beta_{0.5}$ suggests that the value of the TA cutoff frequency in Si, which dictates S1 and affects S2, and the value of s, which dictates S2, are the major factors influencing the spectral contribution to the thermal transport across the interface. To understand this effect, we recalculate $\beta_{0.5}$ after intentionally multiplying the TA branch in Si by a factor of 2. The inset in Fig. 4b depicts this calculation showing that S1 has now been pushed to ~58 Trad s^{-1} and that high frequency phonons are dominant up to this frequency. The inset also shows the corresponding $\alpha(\upsilon_1(\omega_{\max}))$, normalizing $h_K(\upsilon_1(\omega_{\max}))$ at 74 Trad s^{-1}. Going back to α_{qT} in the inset of Fig. 4a, we note that 50% of the computed value is contributed to by 45% of the phonon spectrum in the metal. Given the nearly linear behavior of α_{qT}, this value will not depend on the normalization frequency. Moreover, we note that α_{qT} is a function of the metal properties and is not dependent on S1 or S2. Therefore, the trend and features of $\beta_{0.5}$ are independent of α_{qT} and can be directly associated with $\overline{\zeta_{1\rightarrow2}}$. While α_{qT} affects the magnitude of h_K, the dynamics of phonon transport across the interface are directly related to the transmission coefficient over the entire frequency spectrum.

To further understand how $\overline{\zeta_{1\rightarrow2}}$ dictates the trend seen in $\beta_{0.5}$, and the effect of the frequency modes in the substrate on heat transport across the metal/substrate interface, we measure the thermal boundary conductance across metal/(0001)sapphire

interfaces and compare the value to metal/native oxide/silicon interfaces. The results are shown in Fig. 5. As an aside, the experimental procedures for fabricating and testing these various metal/sapphire interfaces were identical to that discussed in Section III, and each pair of substrates shown in Fig. 5 were coated in the same deposition chamber. It is evident that these metal/sapphire thermal boundary conductance data can be larger (in Al) or smaller (in Pd and Pt) than the metal/Si data even though the "phonon mismatch" is greater by a Debye temperature argument. This suggests that the variation of the magnitude of Kapitza conductance between the two systems, can not be simply interpreted using the "phonon mismatch" idea based on a Debye temperature comparison. As demonstrated in Fig. 4, the dynamics of heat transport across the interface are more complicated and rely on the relative position of the cutoff frequencies in the metal and substrate.

To strengthen our understanding to the role of transmission in thermal transport across the interface, we rearrange Eq. 10 to find that $\overline{\zeta_{1\rightarrow2}\left(\upsilon_1\left(\omega_{\max}\right)\right)}$ is simply a function of h_K and Q_T, represented as

$$\overline{\zeta_{1\rightarrow2}\left(\upsilon_1\left(\omega_{\max}\right)\right)} = \frac{h_\mathrm{K}}{Q_T}. \tag{13}$$

As demonstrated, the thermal boundary conductance measurements on the various samples construct the thermal boundary conductance accumulation function (i.e., the measured data are the quantity h_K). Since we can accurately predict $\partial q_1/\partial T$ (and hence Q_T), we can determine the average phonon transmission in the phonon spectrum of the metal by using the measured TDTR data in Eq. 13. Values for $\overline{\zeta_{1\rightarrow2}}$ for the metal/native oxide/silicon and metal/sapphire are shown in Fig. 6. Note that these values did not require any information about phonon distributions in the substrate. Nevertheless, the quantity shown in Fig. 6a and b, gives direct insight into how phonons couple energy across solid interfaces comprised of silicon with a native oxide layer and sapphire, respectively.

Figure 6a also shows the calculations of $\overline{\zeta_{1\rightarrow2}\left(\upsilon_1\left(\omega_{\max}\right)\right)}$ for metal/silicon interfaces using the assumptions of the DMM. We show acceptable agreement between the DMM calculations and our experimentally derived data of $\overline{\zeta_{1\rightarrow2}\left(\upsilon_1\left(\omega_{\max}\right)\right)}$. Figure 6a shows that $\overline{\zeta_{1\rightarrow2}}$ increases up to S1 and is relatively flat thereafter. Comparing the results in Fig. 6a to the predictions shown in Fig. 4b, we find that the monotonic increase in $\overline{\zeta_{1\rightarrow2}}$ before S1 maintains the high and constant value of $\beta_{0.5}$ before S1. The flattening after S1 results in the reduction and fluctuation of $\beta_{0.5}$ between S1 and S2, and after S2. This result further substantiates that the variation in the spectral contribution to thermal interfacial transport is associated with the transmission coefficient.

The same analysis can be applied to the data Fib. 6b. The steep increase in the calculated transmission coefficient at ~45 Trad s^{-1} suggests that S1 for metal/sapphire system falls somewhere around this frequency. Examining the dispersion curve in sapphire in the $\Gamma \rightarrow Z$, we find that the lowest cutoff frequency in the TA branches occurs at 44 Trad s^{-1} followed by 63 Trad s^{-1} for the cutoff frequency of the LA branch,[113] consistent with our experimental observations of the sharp increase in thermal boundary conductance and calculated average transmission across metal/sapphire interfaces. A more rigorous modeling approach is certainly needed to validate this result in sapphire. We do not attempt to model $\overline{\zeta_{1\rightarrow2}\left(\upsilon_1\left(\omega_{\max}\right)\right)}$ for the metal/sapphire data using the DMM due to the non-cubic crystal structure and additional assumptions that we must apply.[85]

The results in this section agree well with the results in Section II and support our theoretical approach to simulate the Kapitza accumulation for comparison with experimental measurements. The results also provide an additional platform to validate the DMM assumptions of phonon transmissivity beyond simply comparing DMM calculations of h_K to measured data. The model and data agreement in Fig. 6(a) support our assertions in the DMM calculations, namely that phonons scatter diffusively and elastically at metal/native oxide/silicon interfaces. Looking ahead, this approach provides a convenient method to determine average phonon transmissivity across solid interfaces while testing assumptions of phonon scattering at interfaces.

~~The monotonic increase in the temperature derivative of the phonon flux with phonon cutoff frequency, brings to light one of the first conclusions that we find from our accumulation analysis: the magnitudes of thermal boundary conductances across solid interfaces are not necessarily dictated by the "phonon mismatch" of the materials, but are directly correlated to the temperature derivative of the phonon flux impinging on the interface. Accordingly, thermal boundary conductance across interfaces comprised of materials that have a larger phonon mismatch (for example, based on Debye temperature ratio) will not necessarily be smaller than h_K across interfaces that have a smaller mismatch. The actual value of h_K will depend on the phonon flux (energies and velocities).~~

~~Referring back to our discussion regarding α_{qT} in the inset in Fig. 4, the linear increase in the accumulation of this quantity will not change for different substrates. Therefore, the difference between the metal/Si and metal/sapphire data can be attributed to the substrate modes and the average phonon transmission across the interface in the frequency range of the metal phonon spectra, $\overline{\zeta_{1\rightarrow2}\left(\upsilon_1\left(\omega_{\max}\right)\right)}$. For example, our data indicate that the phonon transmission coefficients across metal/native oxide/Si and metal/sapphire interfaces are relatively constant for phonon frequencies greater than ~ 30 Trad s^{-1} and ~ 45 Trad s^{-1}, respectively. This implies that the increase in thermal boundary conductance that is observed when the maximum phonon frequency in the metal goes beyond these two frequencies is due to an increase in phonon flux from high frequency modes and velocities in the metal, and not due to an increase in phonon transmission or better "matching" of the phonon modes near the interface. Thus the change in the metal phonon flux is what dominates interface conductance for high frequency phonons. The fact that $\overline{\zeta_{1\rightarrow2}\left(\upsilon_1\left(\omega_{\max}\right)\right)}$ flattens at 2 different frequencies for Si and sapphire is directly attributed to the substrate modes and~~
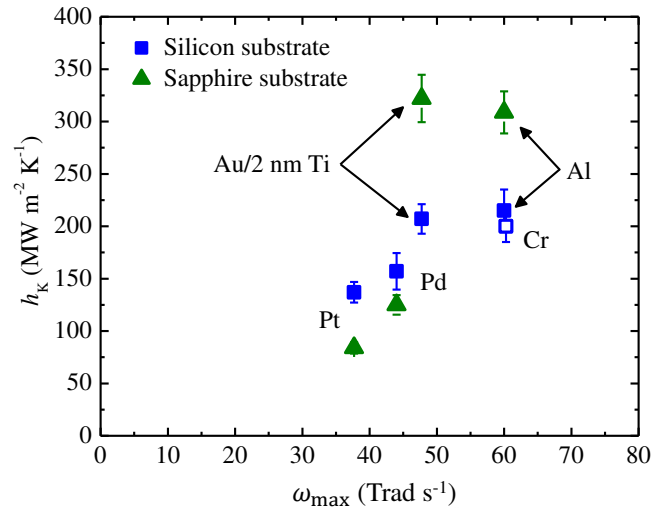
FIG. 5. Measured thermal boundary conductance across various metal/native oxide/Si and metal/sapphire interfaces as a function of metal cutoff frequency. The Cr/Si data point (unfilled square) was taken from Ref. 64 while all other data points (filled symbols) are reported in this work. ~~The measured data show that the magnitude of the thermal boundary conductance across solid interfaces are not necessarily solely driven by the "phonon spectral mismatch", but also are related to the phonon energies and velocities incident on the interface.~~

~~phonon coupling between the metal film and the substrate.~~

V. SUMMARY AND OUTLOOK

In summary, we have developed the analytical theory to calculate the accumulation of phonon thermal boundary conductance as a function of phonon frequency across solid/solid interfaces. Based on the Generalized Mean Value Theorem for definite integrals, we show that this analytical formalism can be related to the average interfacial phonon transmission across interfaces by considering the accumulation of the the temperature derivative of the phonon flux incident upon the interface. We test our theory with a series of thermal boundary conductance measurements across metal/native oxide/silicon and metal/sapphire interfaces. We use the measured values of thermal boundary conductance and calculations of the temperature derivative of the phonon flux to back out a weighted average of the interfacial phonon transmission across the interfaces. Across the metal/native oxide/Si interfaces, we show good agreement with calculations of average spectral phonon transmission predicted from the DMM. We demonstrate that the spectral contribution to the interfacial transport is highly dependent on the relative values of the cutoff frequencies in the two materials comprising the interface. Our approach represents a relatively straight forward method to analyze thermal boundary conductance data across a series of carefully prepared interfaces while quantifying the spectral phonon transmission component to thermal boundary conductance, a quantity that has not been previously measured above superconducting temperatures.

In addition to the advancement in experimental analysis of thermal boundary conductance data and the development of a formalism for frequency accumulation of phonon Kapitza conductance across interfaces, we also report several experimentally supported conclusions that advance the field of phonon interactions at interfaces. ~~As a broad conclusion, we show that the magnitudes of thermal boundary conductances across solid interfaces are not necessarily dictated by the "phonon mismatch" of the materials, but are directly correlated to temperature derivative of the phonon flux impinging on the interface. This interplay between transmission due to phonon mismatch and phonon flux on the magnitude of phonon thermal boundary conductance changes spectrally, and for metal/native oxide/silicon and metal/sapphire interfaces, the phonon transmissivity is flat for high frequency phonons in the substrate, indicating that the changing metal phonon flux dominates the phonon thermal boundary conductance for high frequency phonons.~~ In doing so, we also validate the assumptions of the DMM for metal/native oxide/silicon interfaces based on comparison of the spectrally averaged phonon transmission. In our experimental measurements, we provide measurements of thermal boundary conductance across metal/native oxide/silicon and metal/sapphire interfaces that have not previously been reported. Moreover, we show that for the Au/Ti/Si interface, the influence of phonons in the Ti adhesion layer can affect the thermal boundary conductance for layers as thin as 2 nm. Finally, we demonstrate the utility of TDTR for measuring the thermal conductivity of bulk Si substrates, which further demonstrates the capability of TDTR to
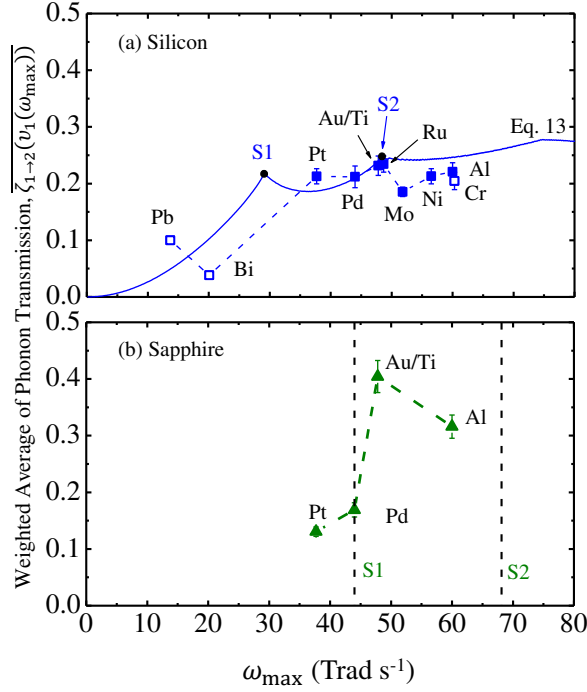
FIG. 6. Average phonon transmission across various (a) metal/native oxide/Si and (b) metal/sapphire interfaces as a function of metal cutoff frequency. The experimental data are derived from Kapitza conductance measurements reported in this work using Eq. 13 and are shown as filled symbols while those derived from previously reported results are depicted as open symbols (Bi and Pb: Ref. 88; Cr: Ref. 64). The solid line in (a) is $\overline{\zeta_{1\to 2}\left(\upsilon_1\left(\omega_{\max}\right)\right)}$ modeled with the DMM. The acceptable agreement between the model and data suggest DMM-like average transmission of phonons across metal/native oxide/silicon interfaces at room temperature. The vertical lines in (b) represent the lowest two cutoff frequencies in sapphire taken from its dispersion curve in the $\Gamma \to Z$ direction[113] and are possible locations for S1 and S2 for the metal/sapphire system.

measure the thermal conductivity of bulk, homogeneous materials with high thermal effusivity.

The utility of this approach lies in the generality in which it was developed. A similar approach can be used with TDTR measurements of thermal boundary conductance across any interface in which this quantity is measurable (i.e., relatively high conductivity substrates). This could be very useful for understanding phonon transmission and interactions across interfaces comprised of a wide array of single crystals, dilute alloys, and some superlattices. When the thermal conductivity of the materials comprising the interface becomes too low, it is difficult to resolve the thermal boundary conductance, so advances in basic metrology must be achieved to extend this approach to low thermal conductivity materials, such as some complex oxides, soft materials (e.g., polymers), amorphous materials, and liquids.

Finally, this study sets the stage for robust theoretical and computational advances in phonon scattering and transmission across interfaces. A more computationally rigorous calculation of phonon flux accounting for the deviation from equilibrium can enhance the accuracy of our model.[114,115] Including contributions due to inelastic scattering processes and using a more realistic dispersion could also account for additional deviations between our model and experimental measurements, especially when using this approach with more complicated interfaces not comprised of a simple metal in which the phonon flux can be relatively well predicted.[19,20,24,116] In addition, it should be possible to study the accumulation of thermal boundary conductance and the average interfacial transmission with molecular dynamics, which could then be used to relate these trends to pure spectral transmission (i.e., not bandwidth averaged). This could provide a systematic computational approach to understand more complex phonon scattering processes such as inelastic scattering[20,21,88,116] or transmission across disordered interfaces,[4] which, when coupled with this experimental approach, will provide great advances in the understanding of phonon transport and thermal conductance in nanosystems.

ACKNOWLEDGMENTS

---

* These authors contributed equally to this work

† phopkins@virginia.edu

[1] D. G. Cahill, W. K. Ford, K. E. Goodson, G. D. Mahan, A. Majumdar, H. J. Maris, R. Merlin, and S. R. Phillpot, Journal of Applied Physics **93**, 793 (2003).

[2] D. G. Cahill, P. V. Braun, G. Chen, D. R. Clarke, S. Fan, K. E. Goodson, P. Keblinski, W. P. King, G. D. Mahan, A. Majumdar, H. J. Maris, S. R. Phillpot, E. Pop, and L. Shi, Applied Physics Reviews **1**, 011305 (2014).

[3] P. M. Norris, N. Q. Le, and C. H. Baker, Journal of Heat Transfer **135**, 061604 (2013).

[4] P. E. Hopkins, International Scholarly Research Notices **2013** (2013), /10.1155/2013/682586.

[5] B. Krenzer, A. Hanisch-Blicharski, P. Schneider, T. Payer, S. Möllenbeck, O. Osmani, M. Kammler, R. Meyer, and M. Horn-vonHoegen, Physical Review B **80**, 024307 (2009).

[6] A. Hanisch, B. Krenzer, T. Pelka, S. Möllenbeck, and M. Horn-vonHoegen, Physical Review B **77**, 125410 (2008).

[7] R. M. Costescu, M. A. Wall, and D. G. Cahill, Physical Review B **67**, 054302 (2003).

[8] P. L. Kapitza, Zhurnal eksperimentalnoi i teoreticheskoi fiziki **11**, 1 (1941).

[9] E. T. Swartz and R. O. Pohl, Reviews of Modern Physics **61**, 605 (1989).

[10] I. M. Khalatnikov, Journal of Experimental and Theoretical Physics (1952).

[11] J. D. N. Cheeke, H. Ettinger, and B. Hebral, Canadian Journal of Physics **54**, 1749 (1976).

[12] R. S. Prasher and P. E. Phelan, Journal of heat transfer **123**, 105 (2001).

[13] N. Q. Le, J. C. Duda, T. S. English, P. E. Hopkins, T. E. Beechem, and P. M. Norris, Journal of Applied Physics **111**, 084310 (2012).

[14] J. C. Duda, J. L. Smoyer, P. M. Norris, and P. E. Hopkins, Applied Physics Letters **95**, 031912 (2009).

[15] T. Beechem, S. Graham, P. Hopkins, and P. Norris, Applied Physics Letters **90**, 054104 (2007).

[16] T. Beechem, J. C. Duda, P. E. Hopkins, and P. M. Norris, Applied Physics Letters **97**, 061907 (2010).

[17] R. S. Prasher and P. E. Phelan, Journal of Heat Transfer **123**, 105 (2001).

[18] P. E. Hopkins and P. M. Norris, Nanoscale and Microscale Thermophysical Engineering **11**, 247 (2007).

[19] P. Reddy, K. Castelino, and A. Majumdar, Applied Physics Letters **87**, 211908 (2005).

[20] P. E. Hopkins, Journal of Applied Physics **106**, 013528 (2009).

[21] P. E. Hopkins, J. C. Duda, and P. M. Norris, Journal of Heat Transfer **133**, 062401 (2011).

[22] J. C. Duda, P. M. Norris, and P. E. Hopkins, Journal of Heat Transfer **133**, 074501 (2011).

[23] C. Dames and G. Chen, Journal of Applied Physics **95**, 682 (2004).

[24] P. E. Hopkins and P. M. Norris, Journal of Heat Transfer **131**, 022402 (2009).

[25] T. Beechem and P. E. Hopkins, Journal of Applied Physics **106**, 124301 (2009).

[26] P. E. Phelan, Journal of Heat Transfer **120**, 37 (1998).

[27] R. S. Prasher, Applied Physics Letters **94**, 041905 (2009).

[28] G. C. Loh, B. K. Tay, and E. H. T. Teo, Applied Physics Letters **97**, 121917 (2010).

[29] G. Chen, Nanoscale Energy Transport and Conversion: A Parallel Treatment of Electrons, Molecules, Phonons, and Photons (Oxford University Press, New York, 2005).

[30] X. Wu and T. Luo, Journal of Applied Physics **115**, 014901 (2014).

[31] R. J. Stevens, L. V. Zhigilei, and P. M. Norris, International Journal of Heat and Mass Transfer **50**, 3977 (2007).

[32] J. C. Duda, T. S. English, E. S. Piekos, W. A. Soffa, L. V. Zhigilei, and P. E. Hopkins, Physical Review B **84**, 193301 (2011).

[33] T. S. English, J. C. Duda, J. L. Smoyer, D. A. Jordan, P. M. Norris, and L. V. Zhigilei, Physical Review B **85**, 035438 (2012).

[34] R. N. Salaway, P. E. Hopkins, P. M. Norris, and R. J. Stevens, International Journal of Thermophysics **29**, 1987 (2008).

[35] X. W. Zhou, R. E. Jones, J. C. Duda, and P. E. Hopkins, Physical Chemistry Chemical Physics **15**, 11078 (2013).

[36] X. W. Zhou, R. E. Jones, C. J. Kimmer, J. C. Duda, and P. E. Hopkins, Physical Review B **87**, 094303 (2013).

[37] R. E. Jones, J. C. Duda, X. W. Zhou, C. J. Kimmer, and P. E. Hopkins, Applied Physics Letters **102**, 183119 (2013).

[38] E. S. Landry and A. J. H. McGaughey, Physical Review B **80**, 165304 (2009).

[39] Z. Y. Ong and E. Pop, Journal of Applied Physics **108**, 103502 (2010).

[40] Z.-Y. Ong and E. Pop, Physical Review B **81**, 155408 (2010).

[41] M. Shen, W. J. Evans, D. Cahill, and P. Keblinski, Physical Review B **84**, 195432 (2011).

[42] L. Hu, L. Zhang, M. Hu, J. S. Wang, B. Li, and P. Keblinski, Physical Review B **81**, 235427 (2010).

[43] M. Hu, P. Keblinski, and P. K. Schelling, Physical Review B **79**, 104305 (2009).

[44] P. K. Schelling, S. R. Phillpot, and P. Keblinski, Applied Physics Letters **80**, 2484 (2002).

[45] W. E. Pickett, J. L. Feldman, and J. Deppe, Modeling and Simulation in Materials Science and Engineering **4**, 409 (1996).

[46] B. C. Daly, H. J. Maris, K. Imamura, and S. Tamura, Physical Review B **66**, 024301 (2002).

[47] S. H. Choi and S. Maruyama, International Journal of Thermal Sciences **44**, 547 (2005).

[48] C.-J. Twu and J.-R. Ho, Physical Review B **67**, 205422 (2003).

[49] A. Maiti, G. Mahan, and S. Pantelides, Solid State Communications **102**, 517 (1997).

[50] F. Yang and C. Dames, Physical Review B **87**, 035437 (2013).

[51] A. J. Minnich, Physical Review Letters **109**, 205901 (2012).

[52] A. S. Henry and G. Chen, Computational and Theoretical Nanoscience **5**, 1 (2008).

[53] K. Esfarjani, G. Chen, and H. T. Stokes, Physical Review B **84**, 085204 (2011).

[54] Z. Tian, J. Garg, K. Esfarjani, T. Shiga, J. Shiomi, and G. Chen, Phys. Rev. B **85**, 184303 (2012).

[55] M. Zebarjadi, K. Esfarjani, M. S. Dresselhaus, Z. F. Ren, and G. Chen, Energy and Environmental Science **5**, 5147 (2012).

[56] K. T. Regner, D. P. Sellan, Z. Su, C. H. Amon, A. J. H. McGaughey, and J. A. Malen, Nature Communications **4**, 1640 (2013).

[57] K. T. Regner, S. Majumdar, and J. A. Malen, Review of Scientific Instruments **84**, 064901 (2013).

[58] Y. K. Koh and D. G. Cahill, Physical Review B **76**, 075207 (2007).

[59] X. Liu, J. L. Feldman, D. G. Cahill, R. S. Crandall, N. Bernstein, D. M. Photiadis, M. J. Mehl, and D. A. Papaconstantopoulos, Physical Review Letters **102**, 035901 (2009).

[60] A. J. Minnich, J. A. Johnson, A. J. Schmidt, K. Esfarjani, M. S. Dresselhaus, K. A. Nelson, and G. Chen, Physical Review Letters **107**, 095901 (2011).

[61] M. E. Siemens, Q. Li, R. Yang, K. A. Nelson, E. H. Anderson, M. M. Murnane, and H. C. Kapteyn, Nature Materials **9**, 26 (2010).

[62] J. C. Duda, C. J. Kimmer, W. A. Soffa, X. W. Zhou, R. E. Jones, and P. E. Hopkins, Journal of Applied Physics **112**, 093515 (2012).

[63] P. M. Norris and P. E. Hopkins, Journal of Heat Transfer **131**, 043207 (2009).

[64] R. J. Stevens, A. N. Smith, and P. M. Norris, Journal of Heat Transfer **127**, 315 (2005).

[65] R. J. Stoner and H. J. Maris, Physical Review B **48**, 16373 (1993).

[66] J. C. Duda, C.-Y. P. Yang, B. M. Foley, R. Cheaito, D. L. Medlin, R. E. Jones, and P. E. Hopkins, Applied Physics Letters **102**, 081902 (2013).

[67] M. D. Losego, M. E. Grady, N. R. Sottos, D. G. Cahill, and P. V. Braun, Nature Materials **11**, 502 (2012).

[68] P. E. Hopkins, M. Baraket, E. V. Barnat, T. E. Beechem, S. P. Kearney, J. C. Duda, J. T. Robinson, and S. G. Walton, Nano Letters **12**, 590 (2012).

[69] C. Y. Ho, R. W. Powell, and P. E. Liley, Journal of Physical and Chemical Reference Data **1**, 279 (1972).

[70] F. Incropera and D. P. DeWitt, Fundamentals of Heat and Mass Transfer, 4th ed. (Wiley and Sons, Inc., New York, 1996).

[71] D. E. Gray, American Institute of Physics Handbook, 3rd ed. (McGraw Hill, New York, 1972).

[72] K. D. Joshi, Calculus for Scientists and Engineers: An Analytical Approach (Narosa, 2002) pp. 448–449.

[73] L. Van Hove, Phys. Rev. **89**, 1189 (1953).

[74] See Supplementary Materials at [URL will be inserted by publisher] for more information.

[75] J. C. Duda, P. E. Hopkins, J. L. Smoyer, M. L. Bauer, T. S. English, C. B. Saltonstall, and P. M. Norris, Nanoscale and Microscale Thermophysical Engineering **14**, 21 (2010).

[76] J. C. Duda, T. Beechem, J. L. Smoyer, P. M. Norris, and P. E. Hopkins, Journal of Applied Physics **108**, 073515 (2010).

[77] J. W. Lynn, H. G. Smith, and R. M. Nicklow, Physical Review B **8**, 3493 (1973).

[78] G. Gilat and R. M. Nicklow, Physical Review **143**, 487 (1966).

[79] W. Weber, Physical Review B **15**, 4789 (1977).

[80] D. P. Sellan, J. E. Turney, A. J. H. McGaughey, and C. H. Amon, Journal of Applied Physics **108**, 113524 (2010).

[81] E. Dechaumphai, D. Lu, J. J. Kan, J. Moon, E. Fullerton, Z. Liu, and R. Chen, Nano letters (2014), 10.1021/nl500127c.

[82] J. B. Hertzberg, M. Aksit, O. O. Otelaja, D. A. Stewart, and R. D. Robinson, Nano Letters **14**, 403 (2014), http://pubs.acs.org/doi/pdf/10.1021/nl402701a.

[83] G. Chen, Applied Physics Letters **82**, 991 (2003).

[84] S. Simons, Journal of Physics C: Solid State Physics **7**, 4048 (1974).

[85] P. E. Hopkins, T. E. Beechem, J. C. Duda, K. Hattar, J. F. Ihlefeld, M. A. Rodriguez, and E. S. Piekos, Physical Review B **84**, 125408 (2011).

[86] P. E. Hopkins, K. Hattar, T. Beechem, J. F. Ihlefeld, D. L. Medlin, and E. S. Piekos, Applied Physics Letters **98**, 231901 (2011).

[87] J. C. Duda and P. E. Hopkins, Applied Physics Letters **100**, 111602 (2012).

[88] H.-K. Lyeo and D. G. Cahill, Phys. Rev. B **73**, 144301 (2006).

[89] P. E. Hopkins, J. C. Duda, C. W. Petz, and J. A. Floro, Physical Review B **84**, 035438 (2011).

[90] P. E. Hopkins, L. M. Phinney, J. R. Serrano, and T. E. Beechem, Physical Review B **82**, 085307 (2010).

[91] C. S. Gorham, K. Hattar, R. Cheaito, T. Beechem, J. C. Duda, J. F. Ihlefeld, D. L. Medlin, E. S. Piekos, and P. E. Hopkins, under review (2014).

[92] A. J. Schmidt, X. Chen, and G. Chen, Review of Scientific Instruments **79**, 114902 (2008).

[93] D. G. Cahill, Review of Scientific Instruments **75**, 5119 (2004).

[94] P. E. Hopkins, J. R. Serrano, L. M. Phinney, S. P. Kearney, T. W. Grasser, and C. T. Harris, Journal of Heat Transfer **132**, 081302 (2010).

[95] C. Thomsen, J. Strait, Z. Vardeny, H. J. Maris, J. Tauc, and J. J. Hauser, Physical Review Letters **53**, 989 (1984).

[96] R. G. Morris and J. G. Hust, Phys. Rev. **124**, 1426 (1961).

97 C. J. Glassbrenner and G. A. Slack, Phys. Rev. **134**, A1058 (1964).

98 D. R. Lide, <u>CRC Handbook for Chemistry and Physics</u>, 89th ed. (Internet Version, CRC Press/Taylor and Francis, Boca Raton, FL, 2008).

99 J. H. Lienhard IV and J. H. Lienhard V, <u>A Heat Transfer Textbook, 4th edition</u> (Courier Dover Publications, 2012).

100 C. Kittel, <u>Introduction to Solid State Physics</u>, 7th ed. (John Wiley and Sons, Inc., New York, 1996).

101 R. Wilson and D. G. Cahill, Nature communications **5** (2014), 10.1038/ncomms6075.

102 G. Chen, Journal of Heat Transfer **119**, 220 (1997).

103 R. Banerjee, R. Ahuja, and H. L. Fraser, Phys. Rev. Lett. **76**, 3778 (1996).

104 B. N. Brockhouse, T. Arase, G. Caglioti, K. R. Rao, and A. D. B. Woods, Physical Review **128**, 1099 (1962).

105 J. Braun, K. Kostov, G. Witte, L. Surnev, J. Skofronick, S. Safron, and C. Wll, Surface Science **372**, 132 (1997).

106 R. J. Birgeneau, J. Cordes, G. Dolling, and A. D. B. Woods, Physical Review **136**, A1359 (1964).

107 D. H. Dutton, B. N. Brockhouse, and A. P. Miller, Canadian Journal of Physics **50**, 2915 (1972).

108 A. P. Miller and B. N. Brockhouse, Canadian Journal of Physics **49**, 704 (1971).

109 W. M. Shaw and L. D. Muhlestein, Physical Review B **4**, 969 (1971).

110 E. D. Murray, S. Fahy, D. Prendergast, T. Ogitsu, D. M. Fritz, and D. A. Reis, Physical Review B **75**, 184301 (2007).

111 Z.-Y. Zeng, C.-E. Hu, L.-C. Cai, X.-R. Chen, and F.-Q. Jing, Journal of Physical Chemistry B **114**, 298 (2010).

112 C. Stassis, D. Arch, B. N. Harmon, and N. Wakabayashi, Physical Review B **19**, 181 (1979).

113 R. Heid, D. Strauch, and K.-P. Bohnen, Phys. Rev. B **61**, 8625 (2000).

114 S. Merabia and K. Termentzidis, Phys. Rev. B **86**, 094303 (2012).

115 J. E. Turney, E. S. Landry, A. J. H. McGaughey, and C. H. Amon, Phys. Rev. B **79**, 064301 (2009).

116 P. E. Hopkins, R. J. Stevens, and P. M. Norris, Journal of Heat Transfer **130**, 022401 (2008).